

A phonon heat bath approach for the atomistic and multiscale simulation of solids

E. G. Karpov^{1,*,†}, H. S. Park^{2,‡} and Wing Kam Liu^{3,§}

¹*Department of Mechanical, Aerospace and Biomedical Engineering, University of Tennessee, Knoxville, TN 37996, U.S.A.*

²*Department of Civil and Environmental Engineering, Vanderbilt University, Nashville, TN 37235, U.S.A.*

³*Department of Mechanical Engineering, Northwestern University, Evanston, IL 60208, U.S.A.*

SUMMARY

We present a novel approach to numerical modelling of the crystalline solid as a heat bath. The approach allows bringing together a small and a large crystalline domain, and model accurately the resultant interface, using harmonic assumptions for the larger domain, which is excluded from the explicit model and viewed only as a hypothetical heat bath. Such an interface is non-reflective for the elastic waves, as well as providing thermostating conditions for the small domain. The small domain can be modelled with a standard molecular dynamics approach, and its interior may accommodate arbitrary non-linearities. The formulation involves a normal decomposition for the random thermal motion term $R(t)$ in the generalized Langevin equation for solid–solid interfaces. Heat bath temperature serves as a parameter for the distribution of the normal mode amplitudes found from the Gibbs canonical distribution for the phonon gas. Spectral properties of the normal modes (polarization vectors and normal frequencies) are derived from the interatomic potential. Approach results in a physically motivated random force term $R(t)$ derived consistently to represent the correlated thermal motion of lattice atoms. We describe the method in detail, and demonstrate applications to one- and two-dimensional lattice structures. Copyright © 2006 John Wiley & Sons, Ltd.

Received 4 November 2005; Revised 8 August 2006; Accepted 10 August 2006

KEY WORDS: heat bath; molecular dynamics; multiscale simulation; crystal structure; normal modes; generalized Langevin equation

*Correspondence to: E. G. Karpov, Department of Mechanical, Aerospace and Biomedical Engineering, University of Tennessee, Knoxville, TN 37996, U.S.A.

†E-mail: ekarpov@utk.edu, edkarpov@gmail.com

‡E-mail: harold.park@vanderbilt.edu

§E-mail: w-liu@northwestern.edu

Contract/grant sponsor: US National Science Foundation

1. INTRODUCTION

During the past decades, there has been a concerted effort in using classical molecular dynamics (MD) simulations for the study of atomic scale phenomena. However, modern atomistic simulations are restricted to very small systems consisting of several million atoms or less and timescales on the order of picoseconds. One possibility to increase the effective size of the system for a reasonable computational cost consists of removing atomic degrees of freedom associated with a bulk ‘heat bath’ region in favour of an effective thermostat, which surrounds a localized region under investigation and maintains heat exchange between the small simulated domain and peripheral media.

A large effort has been made to properly model the mechanism of heat exchange, including the thermostatting approach of Berendsen *et al.* [1]. The basic idea behind the thermostatting approach is to modify the MD equations of motion with a non-conservative friction force, which represents coupling to an external heat bath and scales the atomic velocities on the course of a numerical simulation to add or remove energy from the system as desired. Other approaches applicable for gaseous and liquid domains are the stochastic collisions method of Andersen [2], and the extended systems method originated by Nosé [3] and Hoover [4], which incorporates the external heat bath as an integral part of the system. They accomplished this by assigning the reservoir an additional degree of freedom, and including it in the system Hamiltonian.

The long-term issues associated with the application of heat bath approaches to crystalline solids and polymers, i.e. strongly coupled lattice structures, are the following: (1) energy dissipation is modelled with the viscous friction model, where the frictional force is proportional to the instantaneous atomic velocities; however, energy dissipation in lattice structures is determined by a time history of the atomic motion [5–9]; (2) initial conditions are sampled as independent random quantities, though there is a statistical correlation in the motion of adjacent lattice atoms.

The time-history-dependent energy dissipation can be described by means of the *generalized Langevin equation* (GLE) as follows. Assume that the entire structure under investigation consists of three spatial domains: Ω_P , Ω_I and Ω_Q , see Figure 1. These are the principal domains where a detailed MD solution is sought, the interfacial, and the peripheral (heat bath) domains, respectively. The shape of the interfacial domain Ω_I is determined by the range of an interatomic potential, structural geometry, and a possible atomistic-to-continuum coupling scheme. A common form of the GLE written for atoms in the interfacial region gives [6]

$$m\ddot{x}_{\mathbf{n}}^I = -\frac{\partial U(x^P, x^I, x^Q=0)}{\partial x_{\mathbf{n}}^I} + \sum_{\mathbf{n}'} \int_0^t \beta_{\mathbf{nn}'}(t-\tau) \dot{x}_{\mathbf{n}'}^I(\tau) d\tau + \sum_{\mathbf{n}'} \beta_{\mathbf{nn}'}(t) x_{\mathbf{n}'}^I(0) + R_{\mathbf{n}}^I(t) \quad (1)$$

where the P–I and I–I interactions are assumed harmonic, and x is a component of displacement for an atom associated with the periodic cell of \mathbf{n} in the lattice structure. The bold notation \mathbf{n} stands for a set of integer indices, such as (n) , (n, m) or (n, m, l) used to identify lattice repetitive cells along the interface; examples of this nomenclature are shown in Figure 3. The lattice indices are viewed in the range $n = n_0, \dots, n_0 + N$, $m = m_0, \dots, m_0 + M$, $l = l_0, \dots, l_0 + L$, where n_0 , m_0 , l_0 are some starting values, and values N , M and L refer to the physical dimensions of the lattice along the corresponding directions. Value R is a stochastic function of time that represents the effect of random thermal vibrations. Standard MD equations of motion over the principal domain Ω_P are solved simultaneously with (1). The function U is the system potential energy with the atoms in Ω_Q fixed at their equilibrium positions. β is a component of a large *time-history*

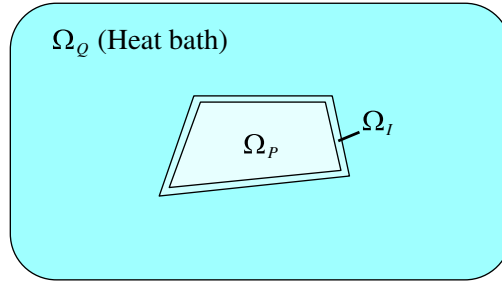


Figure 1. Principal domain of interest Ω_P in thermal contact with a peripheral region Ω_Q . Ω_I is an interfacial region.

kernel (THK) matrix, whose dimension is determined by the number of degrees of freedom in Ω_I . This matrix adequately describes the response of the outer domain Ω_Q due to disturbances in the interfacial domain Ω_I in terms of the I–I correlation.

One important consequence of such a formulation is that propagation of outward progressive waves across the interface in numerical simulations takes place with virtually no artificial reflection. The waves are absorbed by the interface exactly in the same manner, as if the hypothetical domain Ω_Q was *actually* present [6–8]. This feature of the GLE formulation is also valuable for the purpose of multiscale atomistic/continuum simulation using the bridging scale methodology [8, 10–14]. Other approaches incorporating a finite temperature formulation in the multiscale context include the works by Dupuy *et al.* [15], E *et al.* [16], Qu *et al.* [17], Strachan and Holian [18], Curtarolo and Ceder [19], Xiao and Belytschko [20], and Park *et al.* [21].

For a planar interface corresponding to a specific crystallographic direction in the lattice, Equation (1) can be simplified to a form with a compact THK, which is symmetric with respect to translations along the interface. It is also convenient to rewrite the convolution integral in terms of displacement values and separate the I–Q correlation as follows [7–9]:

$$m\ddot{x}_{\mathbf{n}}^I = -\frac{\partial U(x^P, x^I, x^Q)}{\partial x_{\mathbf{n}}^I} \tag{2a}$$

$$x_{\mathbf{n}}^Q = \sum_{\mathbf{n}'} \int_0^t \theta_{\mathbf{n}-\mathbf{n}'}(t-\tau)x_{\mathbf{n}'}^I(\tau) d\tau + R_{\mathbf{n}}^Q(t) \tag{2b}$$

Here, the convolution integral and the random term R in (2b) yield displacement components rather than forces, in contrast with Equation (1). The summation is accomplished along neighbouring lattice cells at the interface only. θ is the compact THK, whose dimension is determined only by the number of degrees of freedom in one repetitive lattice cell; the subscript $\mathbf{n}-\mathbf{n}'$ indicates θ is spatially invariant along the interface, and depends only on the distance between the current and neighbouring cells. Displacements (2b) can be treated as dynamic boundary conditions for the standard MD equation of motion (2a). Such a treatment is convenient for the practical implementation of the GLE methodology into readily available MD codes. In case that the interface Ω_I represents a convex polyhedron, rather than a plane, the treatment (2) is applied separately to all faces of the polyhedron [7, 9].

E and Huang [22] recently proposed a dynamic matching conditions for the coupled atomistic-continuum simulation of solids. The authors introduce a measure of phonon reflection at the interface as a functional over the atomic boundary displacements sought, and find the matching conditions by minimizing the phonon reflection. The present method provides an alternative methodology, which allows also inward flow of thermal energy in its current form, and is based on the time-history integral and lattice Green's function ideas dating back to the works by Adelman and Doll [5, 23].

One important issue that remains open in the GLE formulation (1) or (2) is an appropriate form of the random thermal term R . This term represents time evolution of the atomic force or displacement within the harmonic model given the initial conditions only. Earlier in the literature [5, 23], and also below in this paper (Section 2), an exact expression for R is shown to incorporate atomistic degrees of freedom in the entire heat bath domain; this is intractable in terms of numerical modelling. Furthermore, the random function R cannot be sampled as an independent Gaussian variable at all times, because there is a *correlation* of the thermal noise in lattices in both time and space (see Appendix A.4). This correlation arises due to the coupled nature of crystal lattices, as contrasted to liquids and gases, where the thermal noise is completely uncorrelated. Finally, the term R must represent the canonical ensemble.

These issues can be resolved by the approach proposed in this paper, where the random thermal noise R possesses all the adequate statistical properties imposed by the canonical distribution, including the time/space correlations. The main idea of this approach is in the following. For harmonic lattices, the Hamiltonian can be decoupled in the normal co-ordinates, and the set of lattice normal modes can be viewed formally as a gas of non-interactive quasiparticles, or phonons. Statistical distributions of the random amplitudes and phases of the individual normal modes can be then derived from the Gibbs canonical distribution for the phonon gas at a given temperature T . A linear combination of the normal modes with the random amplitudes and phases provides finally the random displacement term R .

We will focus on the displacement variant of the GLE formulation, and derive systematically an equation similar to (2), though more detailed in terms of practical implementation. Next, we derive semi-analytical expressions for the memory kernel θ and the random displacement function R for a general lattice, using the assumption that the peripheral domain Ω_Q has a uniform temperature field. This implies that Ω_Q is regarded as a heat bath or heat sink, whose temperature and internal energy are not greatly affected by the P-Q heat exchange.

The remainder of the paper is arranged as follows: Sections 2–4 detail with the theoretical aspects of the method. Section 5 provides applications to one- (1D) and two-dimensional (2D) lattice models, and Section 6 concludes the paper.

2. MD BOUNDARY CONDITIONS

In this section, we rewrite boundary conditions (2b) for the generalized Langevin formulation (2) in a form convenient for practical implementation in MD simulations. In the course of our discussion we obtain formal semi-analytical expressions for the THK and a general form of the random displacement term in (2b).

As mentioned in Section 1, the THK describes response of the outer domain Ω_Q due to disturbances originating in the principal domain Ω_P and passing across the interfacial domain Ω_I . An assumption required for a straightforward characterization of the response in the outer domain is

that the interface Ω_I can be comprised by a group of *plane-* or *slab-like* interfaces. Each of these interfaces is to be treated according to the formulation presented below in this paper. Such an assumption, in principle, imposes limitations on allowed shapes of the principal domain, which is expected in the form of a convex polyhedron, though not necessarily regular. See the schematic drawing in Figure 1. Since the principal region is only a *computational* domain, which does not necessarily represent an element of intrinsic physical structure of the solid, this assumption is considered as acceptable. We also require that the outer domain behaves only as a thermostat or heat sink so that *progressive* waves entering Ω_Q are not reflected back by peripheral boundaries of this domain.

A straight line or plane-like boundary can be defined by fixing one of the lattice site indices in the triplet $\mathbf{n} = (n, m, l)$. Due to translational symmetry, we can employ any specific value of this index; the final results will be identical. For example, let $l = 0$. This problem statement corresponds to dividing the entire structure under investigation into the principal, interfacial and bulk peripheral regions in accordance with the following:

$$\Omega_P : l < 0, \quad \Omega_I : l = 0, \quad \Omega_Q : l \geq 1 \tag{3}$$

We will be looking for the bulk domain response only in the immediate vicinity of the interface, i.e. only for atoms $(n, m, 1)$. In other words, our task is to express the displacements vectors $\mathbf{u}_{n,m,1}$ in terms of $\mathbf{u}_{n,m,0}$. We note that the unit (repetitive) cell, denoted by the triplet $\mathbf{n} = n, m, l$, should be chosen large enough, so that atoms in the slab $l = 0$ interact only with atoms in the slab $l = 1$; this requirement is convenient for the purpose of below discussion. Such a unit cell may be represented by the elementary Wigner–Seitz cell, or be comprised of several elementary cells, depending on the range of the lattice potential.

For atoms in the interfacial and peripheral regions, it is convenient to write the linearized equation of motion in the form [10]:

$$M\ddot{\mathbf{u}}_{\mathbf{n}}(t) - \sum_{\mathbf{n}'} \mathbf{K}_{\mathbf{n}-\mathbf{n}'} \mathbf{u}_{\mathbf{n}'}(t) = \mathbf{0}, \quad \mathbf{n} = (n, m, l \geq 0) \tag{4}$$

where $\mathbf{u}_{\mathbf{n}}$ is a vector of displacements of atoms about their equilibrium positions in the unit cell \mathbf{n} . \mathbf{K} are the lattice stiffness matrices, or ‘ K -matrices’, which represent linear elastic properties of the lattice structure. These matrices are comprised of the atomic force constants

$$\mathbf{K}_{\mathbf{n}-\mathbf{n}'} = - \left. \frac{\partial^2 U(\mathbf{u})}{\partial \mathbf{u}_{\mathbf{n}} \partial \mathbf{u}_{\mathbf{n}'}} \right|_{\mathbf{u}=0} \tag{5}$$

where U is the lattice potential written in terms of the atomic displacements. Due to symmetry of the second-order derivative in (5), K -matrices have the following general property:

$$\mathbf{K}_{\mathbf{n}} = \mathbf{K}_{-\mathbf{n}}^T \tag{6}$$

We seek a solution to the boundary value problem governed by (4), where the interfacial displacements $\mathbf{u}_{n,m,0}$ are enforced and known, and the displacements $\mathbf{u}_{n,m,1}$ are to be determined.

An important detail regarding the solution of this problem consists in realizing that the motion of the boundary atoms can be caused either by the displacements of the atoms to be kept, or by an external force acting upon the interfacial atoms in a hypothetical large lattice that extends also for $l < 0$. Therefore, we assume that the motion of the boundary atoms is due to unknown external

forces, which act at $l=0$. Thus,

$$\mathbf{M} \ddot{\mathbf{u}}_{\mathbf{n}}(t) - \sum_{\mathbf{n}'} \mathbf{K}_{\mathbf{n}-\mathbf{n}'} \mathbf{u}_{\mathbf{n}'}(t) = \delta_{l0} \mathbf{f}_{\mathbf{n},m,0} \quad (7)$$

where δ is the Kronecker delta (A10).

Formal application of the Laplace (A4) and discrete Fourier transforms (DFTs) (A11) to Equation (7) gives

$$\hat{\mathbf{U}}(\mathbf{p}, \alpha) = \hat{\mathbf{G}}(\mathbf{p}, \alpha) \hat{\mathbf{F}}_0(\mathbf{p}, \alpha) + \hat{\mathbf{R}}(\mathbf{p}, \alpha) \quad (8)$$

$$\hat{\mathbf{G}}(\mathbf{p}, \alpha) = (\alpha^2 \mathbf{M} - \hat{\mathbf{K}}(\mathbf{p}))^{-1} \quad (9)$$

$$\hat{\mathbf{R}}(\mathbf{p}, \alpha) = \mathbf{M} \hat{\mathbf{G}}(\mathbf{p}, \alpha) (\alpha \hat{\mathbf{u}}(\mathbf{p}, 0) + \dot{\hat{\mathbf{u}}}(\mathbf{p}, 0)) \quad (10)$$

where the transformed force, $\hat{\mathbf{F}}_0(\mathbf{p}, \alpha) \equiv \hat{\mathbf{F}}_0(p, q, \alpha)$. Substitution of this force into (8) and further application of the inverse DFT over $r \rightarrow l$ lead to

$$\tilde{\mathbf{U}}_l(p, q, \alpha) - \tilde{\mathbf{R}}_l(p, q, \alpha) = \tilde{\mathbf{G}}_l(p, q, \alpha) \hat{\mathbf{F}}_0(p, q, \alpha) \quad (11)$$

Here, the tilde notation stands for the mixed (transform/real space) quantities that depend on l and the transform variables p, q and α . The force vector $\hat{\mathbf{F}}_0$ can be eliminated by writing two equations (11), for $l=0$ and 1, and substituting $\hat{\mathbf{F}}_0$ from the first of these equations into the second:

$$\tilde{\mathbf{U}}_1(p, q, \alpha) - \tilde{\mathbf{R}}_1(p, q, \alpha) = \tilde{\mathbf{\Theta}}(p, q, \alpha) (\tilde{\mathbf{U}}_0(p, q, \alpha) - \tilde{\mathbf{R}}_0(p, q, \alpha)) \quad (12)$$

$$\tilde{\mathbf{\Theta}}(p, q, \alpha) = \tilde{\mathbf{G}}_1(p, q, \alpha) \tilde{\mathbf{G}}_0^{-1}(p, q, \alpha) \quad (13)$$

Finally, application of the inverse DFT transform (A14) over $p \rightarrow n$ and $q \rightarrow m$, and the inverse Laplace transform onto (12) result in a solution of the form

$$\mathbf{u}_{n,m,1}(t) = \sum_{n',m'} \int_0^t d\tau \theta_{n-n',m-m'}(t-\tau) (\mathbf{u}_{n',m',0}(\tau) - \mathbf{R}_{n',m',0}(\tau)) + \mathbf{R}_{n,m,1}(t) \quad (14)$$

In this expression

$$\theta_{n,m}(t) = \mathcal{L}_{\alpha \rightarrow t}^{-1} \mathcal{F}_{p \rightarrow n}^{-1} \mathcal{F}_{q \rightarrow m}^{-1} \{ \tilde{\mathbf{G}}_1(p, q, \alpha) \tilde{\mathbf{G}}_0^{-1}(p, q, \alpha) \} \quad (15a)$$

$$\tilde{\mathbf{G}}_l(p, q, \alpha) = \mathcal{F}_{r \rightarrow l}^{-1} \{ \hat{\mathbf{G}}(\mathbf{p}, \alpha) \}, \quad \mathbf{p} \equiv (p, q, r) \quad (15b)$$

where the symbols \mathcal{F}^{-1} and \mathcal{L}^{-1} stand for the inverse DFT and Laplace transform, respectively. The vector \mathbf{R} depends on the initial conditions (the capital letter \mathbf{R} is used for both Laplace and time domain functions)

$$\mathbf{R}_{\mathbf{n}}(t) = \mathbf{M} \sum_{\mathbf{n}'} (\mathbf{g}_{\mathbf{n}-\mathbf{n}'}(t) \dot{\mathbf{u}}_{\mathbf{n}'}(0) + \mathbf{g}_{\mathbf{n}-\mathbf{n}'}(t) \mathbf{u}_{\mathbf{n}'}(0)) \quad (16a)$$

$$\mathbf{g}_{\mathbf{n}}(t) = \mathcal{L}_{\alpha \rightarrow t}^{-1} \mathcal{F}_{p \rightarrow n}^{-1} \mathcal{F}_{q \rightarrow m}^{-1} \mathcal{F}_{r \rightarrow l}^{-1} \{ \hat{\mathbf{G}}(\mathbf{p}, \alpha) \} \quad (16b)$$

The time-dependent matrix function \mathbf{g} is known as the lattice dynamics Greens function [7, 10]. This function describes response of a large, non-constrained lattice to localized unit excitations, or localized perturbations of initial conditions.

Solution (14) can serve as a boundary condition to the MD equation of motion (2a), provided that the atoms in a given plane or slab of constant l interact only with each other and with atoms in the adjacent slabs $l - 1$ and $l + 1$. For longer ranged forces, the size of the unit cell must be increased so that this requirement is satisfied. At the same time, range of the interaction along the directions n and m can be arbitrary. Boundary conditions of the type (15)–(16) were also discussed in [7, 9] with the assumptions that the interface is initially at rest, and temperature of the external region is zero at all times; within these settings, $\mathbf{R}_n(t) = \mathbf{0}$.

Below we rewrite the boundary condition (14) in the sample extended forms corresponding to 1D, 2D and 3D lattices, respectively:

$$\mathbf{u}_1(t) = \int_0^t \boldsymbol{\theta}(t - \tau)(\mathbf{u}_0(\tau) - \mathbf{R}_0(\tau)) d\tau + \mathbf{R}_1(t), \quad \Omega_1 : n = 0 \tag{17a}$$

$$\mathbf{u}_{n,1}(t) = \sum_{n'=n-n_c}^{n+n_c} \int_0^t d\tau \boldsymbol{\theta}_{n-n'}(t-\tau)(\mathbf{u}_{n',0}(\tau) - \mathbf{R}_{n',0}(\tau)) + \mathbf{R}_{n,1}(t), \quad \Omega_1 : m = 0 \tag{17b}$$

$$\begin{aligned} \mathbf{u}_{n,m,1}(t) = & \sum_{n'=n-n_c}^{n+n_c} \sum_{m'=m-m_c}^{m+m_c} \int_0^t d\tau \boldsymbol{\theta}_{n-n',m-m'}(t - \tau) \\ & \times (\mathbf{u}_{n',m',0}(\tau) - \mathbf{R}_{n',m',0}(\tau)) + \mathbf{R}_{n,m,1}(t), \quad \Omega_1 : l = 0 \end{aligned} \tag{17c}$$

For most potentials, it is proper to truncate the convolution sums at $n_c, m_c = 4 \dots 6$; such a truncation can significantly reduce computational cost of these boundary condition [7].

The boundary conditions in one of the forms (17) are convenient for practical implementation, because the THK (15) has a compact size of $S \times S$, where S is the number of degrees of freedom in one unit cell only. Furthermore, matrix $\boldsymbol{\theta}$ is a fundamental structural characteristic of the periodic lattice; it is unique for a given lattice model and a specific crystallographic plane. This plane is coplanar with the interface Ω_1 . The THK relates the displacement solution in Ω_Q with the localized boundary perturbations. The physical meaning of the kernel $\boldsymbol{\theta}$ is explained in Figure 2. Numerical evaluation of the time history kernel (15) is straightforward by utilizing the numerical methods for Laplace and DFT inversion, which are reviewed in the Appendix.

3. NORMAL MODE REPRESENTATION OF THE RANDOM NOISE

There are three important observations regarding the original structure of random displacement term \mathbf{R} , Equation (16), in the boundary conditions (17). First, it requires expensive evaluation of the lattice Green's function \mathbf{g} over the entire structure including the hypothetical heat bath region. Second, it requires knowledge of initial conditions for all atoms, such that the lattice is found in thermodynamic equilibrium at a given heat bath temperature T . Both of these requirements make direct usage of the formulation impractical.

Meantime, the third observation is crucial in the sense that it allows resolving the first two issues in a numerically tractable manner: in fact, the random vector (16) *satisfies the homogeneous*

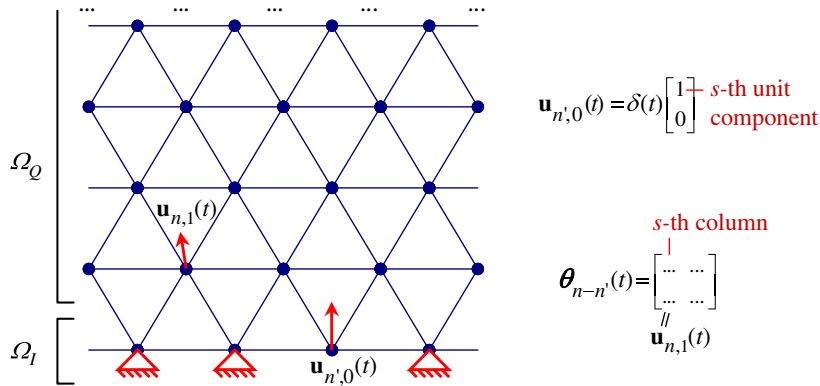


Figure 2. The s th column of kernel matrix θ shows the vector of displacements for the current cell $(n, 1)$, due to the s th unit component of a boundary displacement vectors at $(n', 0)$, with the rest of boundary being fixed.

equation of motion (4). Indeed, for a zero external force vector $\hat{\mathbf{F}}$ in the right-hand side of Equation (8), one obtains

$$\hat{\mathbf{U}}(\mathbf{p}, \alpha) = \hat{\mathbf{R}}(\mathbf{p}, \alpha) \tag{18}$$

The above observation is important for the following reasons. Assume that the heat bath Ω_Q is in thermal equilibrium at $t = 0$. Then the initial conditions in (16a), and therefore the vector \mathbf{R} , can be associated with the *equilibrium* thermal motion only. Indeed, all non-equilibrium, non-random effects in Ω_Q are described by the kernel matrix θ in (14) or (17). The equilibrium oscillations, imposing no energy transfer across the interface, can be most naturally represented by the *normal mode* solutions to Equation (8), i.e. by a superposition of free-standing waves in the lattice structure. These solutions has been well studied in literature, e.g. [10, 24, 25]. With the present notations, the normal mode representation gives [10]

$$\mathbf{R}_n(t) = \mathbf{u}_n^+(t) + \mathbf{u}_n^-(t) \tag{19}$$

where \mathbf{u}^\pm are the real-valued vectors

$$\mathbf{u}_n^+(t) = \sum_{\mathbf{p},s} a_{\mathbf{p},s}^+ \cos(\omega_{\mathbf{p},s}t + \phi_{\mathbf{p},s}^+) (\cos(\tilde{\mathbf{p}} \cdot \mathbf{n}) \text{Re } \mathbf{d}_{\mathbf{p},s} - \sin(\tilde{\mathbf{p}} \cdot \mathbf{n}) \text{Im } \mathbf{d}_{\mathbf{p},s}) \tag{20a}$$

and

$$\mathbf{u}_n^-(t) = \sum_{\mathbf{p},s} a_{\mathbf{p},s}^- \cos(\omega_{\mathbf{p},s}t + \phi_{\mathbf{p},s}^-) (\sin(\tilde{\mathbf{p}} \cdot \mathbf{n}) \text{Re } \mathbf{d}_{\mathbf{p},s} + \cos(\tilde{\mathbf{p}} \cdot \mathbf{n}) \text{Im } \mathbf{d}_{\mathbf{p},s}) \tag{20b}$$

where $\tilde{\mathbf{p}} = 2\pi(p/N, q/M, r/L)$, and $\mathbf{p} = (p, q, r)$ is a vector of integer wave numbers. The operators Re and Im give the real and imaginary parts of the polarization vectors \mathbf{d} determined by the parametric eigenvalue problem

$$-\mathbf{M}^{-1} \hat{\mathbf{K}}(\mathbf{p}) \mathbf{d}_{\mathbf{p},s} = \omega_{\mathbf{p},s}^2 \mathbf{d}_{\mathbf{p},s} \tag{21}$$

with a symmetry with respect to the complex conjugation

$$\mathbf{d}_{\mathbf{p},s}^* = \mathbf{d}_{-\mathbf{p},s} \tag{22}$$

The index s numbers different dispersion branches, i.e. various solutions of the characteristic equation

$$\det(\omega^2 \mathbf{M} + \hat{\mathbf{K}}(\mathbf{p})) = 0 \tag{23}$$

There are in total S dispersion branches, where S is the number of degrees of freedom in the lattice unit cell.

The normal amplitudes and phases can be different in (20a) and (20b) for the same pair \mathbf{p} and s , however, they should satisfy

$$a_{-\mathbf{p},s}^+ = a_{\mathbf{p},s}^+, \quad a_{-\mathbf{p},s}^- = -a_{\mathbf{p},s}^-, \quad \phi_{-\mathbf{p},s}^\pm = \phi_{\mathbf{p},s}^\pm \tag{24}$$

Due to symmetries (22) and (24), any pair of terms in (20a) or (20b) corresponding to $-\mathbf{p}$ and \mathbf{p} are identical. Thus, solutions (20) are comprised in total by SN_c , $N_c = NML$, linearly independent real-valued normal modes. Note that the value SN_c is equal to the total number of vibrational and translational degrees of freedom in the lattice structure. Obviously, any linear combination of (20a) and (20b) will also satisfy the governing equation (4).

We note that before the disturbance from the MD domain Ω_p reaches the interface, the interface is at thermal equilibrium, and we may assume that $\mathbf{u}_0 = \mathbf{R}_0$. Then the boundary conditions (17) yield $\mathbf{u}_1 = \mathbf{R}_1$, which agrees with the physical arguments behind formula (19).

Usage of the random displacement vector in the form (19) is much more effective computationally, as compared to (16). Relationships (19) and (20) represent a key element of the proposed methodology. Further practical issues, including truncation of the sums in (20) are discussed in Section 4.

3.1. Normal amplitudes and phases: statistical properties

Free parameters of the normal mode solution (20), the normal amplitudes and phases, can be chosen arbitrary, so that the lattice motion satisfies initial conditions, or meets specific thermodynamic characteristics. One such characteristic can be the equilibrium temperature T .

There are in total $2SN_c$ free parameters: SN_c normal amplitudes a and SN_c phases ϕ ; S is the number of degrees of freedom per lattice unit cell, and N_c is the total number of unit cells. We can derive these amplitudes and phases in a probabilistic manner only from the knowledge of the lattice temperature T and lattice spectral properties, i.e. the normal frequencies and polarization vectors. For this purpose we utilize the Gibbs canonical distribution

$$W = \frac{1}{Z} \exp\left(-\frac{H}{k_B T}\right) \tag{25}$$

which encapsulates statistical properties of a classical multiparticle system in thermodynamic equilibrium at constant temperature T and constant number of particles [10, 26–28]. Here, H is the system Hamiltonian, Z a normalization factor, and k_B the Boltzmann constant. The linearized Hamiltonian of a periodic lattice structures reads as

$$H = \frac{1}{2} \sum_{\mathbf{n}} \dot{\mathbf{u}}_{\mathbf{n}}^T \mathbf{M} \dot{\mathbf{u}}_{\mathbf{n}} - \frac{1}{2} \sum_{\mathbf{n}, \mathbf{n}'} \mathbf{u}_{\mathbf{n}}^T \mathbf{K}_{\mathbf{n}-\mathbf{n}'} \mathbf{u}_{\mathbf{n}'} \tag{26}$$

Substituting displacements (20) into this relationship and further averaging in time yields

$$H = \frac{N_c}{2} \sum_{\mathbf{p},s} a_{\mathbf{p},s}^2 \chi_{\mathbf{p},s} = \frac{N_c}{2} \sum_{\mathbf{p},s} a_{\mathbf{p},s}^2 \omega_{\mathbf{p},s}^2 \mu_{\mathbf{p},s} \quad (27)$$

Here, we introduced the characteristic mass and stiffness of the normal mode

$$\mu_{\mathbf{p},s} = \mathbf{d}_{\mathbf{p},s}^\dagger \mathbf{M} \mathbf{d}_{\mathbf{p},s}, \quad \chi_{\mathbf{p},s} = -\mathbf{d}_{\mathbf{p},s}^\dagger \hat{\mathbf{K}}(\mathbf{p}) \mathbf{d}_{\mathbf{p},s} \quad (28)$$

which are related to the normal frequency as

$$\omega_{\mathbf{p},s}^2 = \chi_{\mathbf{p},s} / \mu_{\mathbf{p},s} \quad (29)$$

The dagger symbol in (28) stands for a complex conjugate and transposed vector. Thus, complex lattice vibrations in the space of wave numbers can be regarded as a result of the oscillatory motion of SN_c quasiparticles, characterized by the mass μ and stiffness χ in accordance with (28). These quasiparticles are called the lattice *phonons*, and a complete set of phonons for a given lattice domain comprise a formal system known as the phonon gas.

For a harmonic lattice the phonon gas is non-interactive, as a result, the Hamiltonian (27) is additive, where the total energy is given as a sum of the energies of the individual normal nodes. For an additive Hamiltonian, the Gibbs distribution is factorized, and we can find statistical distributions of the normal amplitude and phase of the *individual* normal modes. For this purpose, we note that each pair of the random quantities $(a_{\mathbf{p},s}, \phi_{\mathbf{p},s})$ determines polar co-ordinates of a point in the formal configuration space associated with the normal mode (\mathbf{p}, s) . In order to obtain statistical distributions for a and ϕ , we substitute expression (27) into (25) and multiply the result by the elementary volume $a_{\mathbf{p},s} da_{\mathbf{p},s} d\phi_{\mathbf{p},s}$

$$dW = \frac{1}{Z} \prod_{\mathbf{p},s} a_{\mathbf{p},s} \exp \frac{-N_c a_{\mathbf{p},s}^2 \omega_{\mathbf{p},s}^2 \mu_{\mathbf{p},s}}{2k_B T} da_{\mathbf{p},s} d\phi_{\mathbf{p},s} \quad (30)$$

This equation represents an infinitesimal probability in the (a, ϕ) -space. It indicates that the normal amplitudes and phases are independent random variables distributed according to

$$w(a_{\mathbf{p},s}) = \frac{N_c a_{\mathbf{p},s} \omega_{\mathbf{p},s}^2 \mu_{\mathbf{p},s}}{k_B T} \exp \frac{-N_c a_{\mathbf{p},s}^2 \omega_{\mathbf{p},s}^2 \mu_{\mathbf{p},s}}{2k_B T} \quad (31a)$$

$$w(\phi_{\mathbf{p},s}) = \frac{1}{2\pi} \quad (31b)$$

The phases are distributed uniformly in the interval $(0, 2\pi)$. As follows from (31a), the mean square amplitude is

$$\langle a_{\mathbf{p},s}^2 \rangle = \int_0^\infty a_{\mathbf{p},s}^2 w(a_{\mathbf{p},s}) da_{\mathbf{p},s} = \frac{2k_B T}{N_c \omega_{\mathbf{p},s}^2 \mu_{\mathbf{p},s}} \quad (32)$$

On the basis of (27) and (32), we may also obtain the mean energy of an individual mode

$$\langle \varepsilon_{\mathbf{p},s} \rangle = \frac{N_c}{2} \langle a_{\mathbf{p},s}^2 \rangle \omega_{\mathbf{p},s}^2 \mu_{\mathbf{p},s} = k_B T \quad (33)$$

where T is the equilibrium heat bath temperature. Remarkably, this energy is invariant for all normal modes, and for all types of harmonic lattices. This result is in agreement with the equipartition theorem of statistical mechanics [26–28], proving distributions (31) to be consistent from the energetic point of view.

4. SUMMARY OF THE METHOD

The purpose of this section is to provide a brief summary of those elements that are important in terms of practical usage for the proposed method.

The most important practical result of this method are the boundary conditions (17), where the random displacement vector is chosen in the form of a normal mode decomposition, Equations (19) and (20). These boundary conditions are applied along planar interfaces of a simulation domain, incorporating the regions Ω_P and Ω_I , see Figure 1 or 2. The free parameters of decomposition (20), the normal amplitudes and phases, are sampled from the statistical distributions (31) *once only*—at the initial time step of the simulation. At the successive time steps, the random displacement vector \mathbf{R} is evaluated using the normal mode decomposition (20), where a relevant value of the time variable is utilized; meantime, the random phases and amplitudes are kept invariant at all time steps. The distribution of normal amplitudes (31a) utilizes knowledge of the lattice spectral properties encapsulated by the normal frequencies (23), polarization vectors (21) and characteristic masses (28). The temperature T involved in this distribution is regarded as the heat bath, or target system, temperature.

Provided that there is no input or release of energy inside Ω_P or Ω_I , temperature in these domains will be approaching the value T utilized for the amplitudes (32). At the same time, the convolution integral in the boundary conditions (17) will be damping all the non-equilibrium oscillations, represented by the difference $(u_0 - R_0)$, and the displacements u_1 will be approaching R_1 in a stochastic manner. In thermal equilibrium, statistical properties of the displacement vector on the interface will be identical with the statistical properties of the vector \mathbf{R} that corresponds to a canonical ensemble by the definition. In general, the mechanism of heat exchange will be identical as in a hypothetical simulation incorporating atomistic resolution over the entire peripheral domain Ω_Q . Furthermore, since the interfacial atoms behave as if they were a part of the large hypothetical domain Ω_Q in equilibrium at a given temperature, the principal domain Ω_P will correspond to a canonical ensemble, if found in thermodynamic equilibrium with Ω_Q .

In terms of dissipation of elastic (shock) waves and heat, the domain Ω_Q is *infinite*, in principle. Propagation of long elastic waves in a peripheral domain with a specific *finite* geometry, can be incorporated via joint usage of this method with a hybrid MD/FEM methodology [10, 29], in particular, with the bridging scale method [10, 12–14, 30, 31]. Within the bridging scale approach, the temperature-dependent boundary conditions of the type (17) can be applied to the fine scale displacement field at an interface between the atomistic and continuum regions.

Equilibrium MD initial conditions for Ω_I and a periodic part of Ω_P can be obtained simply as

$$\mathbf{u}_n(0) = \mathbf{R}_n(0), \quad \dot{\mathbf{u}}_n(0) = \dot{\mathbf{R}}_n(0) \quad (34)$$

These initial conditions automatically account for the statistical correlation between the positions and velocities of neighbouring atoms within a strongly coupled system, such as the crystal lattice (see Appendix A.4). As a result, the random phase space vector provided by (34) is compliant

Table I. Summary of the method.

Geometry and elastic properties	Spectral and statistical properties	MD boundary conditions
(5) $\rightarrow \mathbf{K}_{\mathbf{n}}$	(23) $\rightarrow \omega_{\mathbf{p},s}$ (21) $\rightarrow \mathbf{d}_{\mathbf{p},s}$ (31) $\rightarrow a_{\mathbf{p},s}, \phi_{\mathbf{p},s}$	(15) $\rightarrow \boldsymbol{\theta}_{n,m}(t)$ (17) $\rightarrow \mathbf{u}_{n,m,1}(t)$ (19) $\rightarrow \mathbf{R}_{\mathbf{n}}(t)$

with the Gibbs canonical distribution (25), and provides a physically adequate ‘snapshot’ of the lattice in thermodynamic equilibrium with the heat bath. In other words, conditions (34) represent a typical microscopic state of a periodic lattice at temperature T .

In order to save computational effort in practical applications, the total number of modes used for decompositions (20) can be chosen less than SN_c . For example, the low-frequency part of the spectrum may require truncation, when the period of vibration for the corresponding modes become comparable with the total time of the MD simulation. A further decrease in the number of modes can be achieved by increasing the sampling interval for the wavenumbers in (20); for example, the wavenumbers can be sampled from $\pm\pi/2$ to $\pm\pi$ with a constant step π/z , where z is integer. In all cases, the parameter N_c in (31a) and (32) must be replaced with the total number of distinct wavenumber triplets $\mathbf{p} = (p, q, r)$ employed. Since any decrease in the number of modes will abate the initial entropy of the system, it is desirable in numerical simulations to keep a large yet reasonable number of normal modes.

In order to achieve an accurate target temperature in the case of a limited number of modes (less than 10^3), one may compute the normal amplitudes for (20) simply as square roots of the mean values (32), rather than sampling them from the original distribution (31a) in a probabilistic manner. The phases of the normal modes in decomposition (20) must be randomly sampled in all instances, as values uniformly distributed over $[0, 2\pi]$. Recall that the normal amplitudes and phases are pre-evaluated once only for an entire simulation run. Then, formulas (19) and (20) are used to evaluate the vector \mathbf{R} for any arbitrary physical time (time step) of the simulation.

We can summarize that implementation of the present formulation is comprised of three successive steps, see Table I: (1) analysis of lattice geometry and evaluation of elastic properties in the form of K -matrices, (2) evaluation of spectral properties of the lattice, and (3) construction of the boundary conditions. These steps are programmed in a preliminary block of a MD code, or resolved analytically when possible. Specific examples and some useful numerical strategies are discussed in Section 5.

5. ANALYTICAL AND NUMERICAL EXAMPLES

In this section, we demonstrate practical aspects of the method in application to a 1D monoatomic chain and 2D hexagonal lattice, both with the nearest neighbour interaction. The corresponding associate substructures are shown in Figure 3. The associate substructure fully represents the mechanical properties of a periodic lattice, including the spectral and response characteristics; it is comprised of an arbitrary (current) unit cell, (n) or (n, m) in Figure 3, and all neighbouring cells interacting directly with the current cell.

The chain lattice is unique in terms of the possibility to evaluate all spectral and response properties, along with the THK, in closed-form. The hexagonal lattice allows closed-form

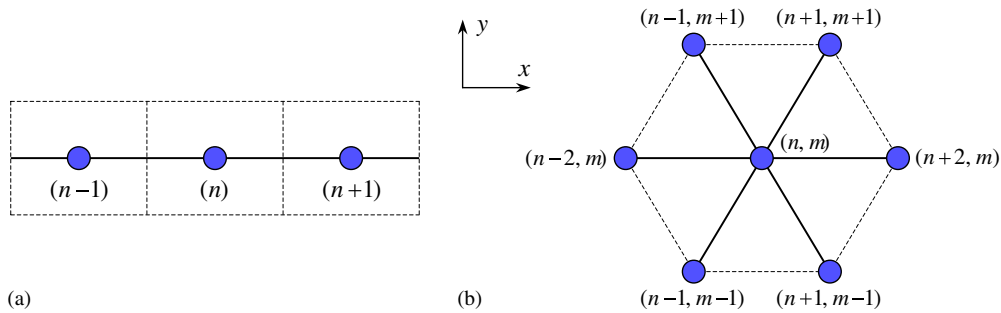


Figure 3. Associate substructures of chain-like (left) and hexagonal (right) lattices with the nearest neighbour interactions.

evaluation of only the spectral properties and the K -matrices. For more complex structures, all lattice characteristics are evaluated numerically on the basis of an interatomic potential. The spectral characteristics are found from (23), (21) and (28) for each specific wave vector \mathbf{p} and branch number s of interest. The THK is evaluated numerically on the basis of (15).

Note that the K -matrices (5) serve as input for the THK evaluation, and they can be computed numerically as well. Numerical computation of the K -matrices is particularly reasonable for complex interatomic potentials, when the second-order derivatives of the lattice potential U in (5) are analytically cumbersome (even though U is written for the associate substructure only). Various methods for numerical computation of second-order derivatives of complex functions can be found elsewhere in literature; special techniques accounting for the specifics of the lattice structure application are discussed in [32].

5.1. 1D lattice in thermal equilibrium

Consider application of the proposed heat bath approach to the monoatomic lattice chain, Figure 3(a), comprised of $N_a = 1001$ atoms with one longitudinal degree of freedom. Obviously, the number of atoms N_a and the number of unit cells N_c are identical for this lattice. The lattice is governed by the pairwise Morse potential with the Au (gold) parameters [33]

$$V(r) = \varepsilon(e^{2\beta(\rho-r)} - 2e^{\beta(\rho-r)}), \quad \varepsilon = 0.560 \text{ eV}, \quad \beta = 1.637 \text{ \AA}^{-1}, \quad \rho = 2.922 \text{ \AA} \quad (35)$$

and a cut-off radius of 1.5ρ . Thus, each lattice atom interacts with two nearest neighbours only, and the value ρ gives the equilibrium interatomic distance. In our numerical computations we utilize 1 eV, 1 ps and 1 Å as the units of energy, time and length. Then, the mass unit is given by $1 \text{ eV} \times 1 \text{ ps}^2 \times 1 \text{ \AA}^{-2} = 1.602 \times 10^{-23} \text{ kg}$. In these units, the mass of one Au atom and the Boltzmann constant are

$$m = 0.02042, \quad k_B = 8.6183 \times 10^{-5} \quad (36)$$

Temperature is still expressed in Kelvin (K).

Below, we show all successive steps for the derivation of the random vector \mathbf{R} , and the THK θ for the boundary condition (17a). As mentioned, all these steps are possible for the chain lattice

in closed form, involving only the physical parameters from (35) and (36), and the heat bath temperature T .

1. *Equilibrium positions and co-ordinates* of lattice atoms along the x -axis:

$$\mathbf{e}_n = \rho n, \quad \mathbf{r}_n(t) = \mathbf{e}_n + \mathbf{u}_n(t) = \rho n + \mathbf{u}_n(t) \quad (37)$$

Here, \mathbf{u}_n is the displacement of the atom n ; this is a one-component vector (scalar) for the monoatomic unit cell with a single degree of freedom per atom.

2. *Potential energy* of the lattice written for one associate cell, Figure 3(a), in terms of the atomic displacements:

$$\begin{aligned} U(\mathbf{u}) &\equiv U(\mathbf{u}_{n-1}, \mathbf{u}_n, \mathbf{u}_{n+1}) = V(\mathbf{r}_n - \mathbf{r}_{n-1}) + V(\mathbf{r}_{n+1} - \mathbf{r}_n) \\ &= V(\mathbf{u}_n - \mathbf{u}_{n-1} + \rho) + V(\mathbf{u}_{n+1} - \mathbf{u}_n + \rho) \end{aligned} \quad (38)$$

Here, V is the Morse potential (35).

3. *K-matrices* (5):

$$\mathbf{K}_0 = - \left. \frac{\partial^2 U(\mathbf{u})}{\partial^2 \mathbf{u}_n} \right|_{\mathbf{u}=0} = -4\varepsilon\beta^2, \quad \mathbf{K}_{-1} = \mathbf{K}_1 = - \left. \frac{\partial^2 U(\mathbf{u})}{\partial \mathbf{u}_n \partial \mathbf{u}_{n+1}} \right|_{\mathbf{u}=0} = 2\varepsilon\beta^2 \quad (39)$$

where ε and β are the Morse parameters (35). The notation $\mathbf{u}=0$ means that we employ $\mathbf{u}_{n-1} = \mathbf{u}_n = \mathbf{u}_{n+1} = 0$ after the second-order derivatives are obtained. Notice that $\mathbf{K}_n = 0$ at $|n| > 1$. Also note that for the nearest neighbour interaction model, the value $2\varepsilon\beta^2$ represents the linear stiffness constant of the interaction between two adjacent atoms

$$k = 2\varepsilon\beta^2 = 3.0013 \text{ eV}/\text{\AA}^2 \quad (40)$$

4. *DFT (A11) of the K-matrices*:

$$\hat{\mathbf{K}}(p) = \sum_n \mathbf{K}_n e^{-ipn} = \mathbf{K}_{-1} e^{ip} + \mathbf{K}_0 + \mathbf{K}_1 e^{-ip} = k(e^{ip} - 2 + e^{-ip}) = 2k(\cos p - 1) \quad (41)$$

5. *Normal frequencies* (23):

$$(\omega^2 m + \hat{\mathbf{K}}(p)) = 0 \rightarrow \omega_p = \Omega \sin \frac{p}{2}, \quad \Omega = 2\sqrt{k/m} \quad (42)$$

6. *Polarization vectors* (21):

$$-m^{-1} \hat{\mathbf{K}}(p) \mathbf{d}_p = \omega_p^2 \mathbf{d}_p \rightarrow \omega_p^2 \mathbf{d}_p = \omega_p^2 \mathbf{d}_p \rightarrow \mathbf{d}_p = 1 \quad (43)$$

The one-component vector \mathbf{d}_p is a constant independent of p . In general, the polarization vectors must be normalized, therefore we utilize $\mathbf{d}_p = 1$.

7. *Characteristic masses* (28):

$$\mu_p = m \quad (44)$$

8. *Normal amplitudes* (32):

$$a_p = \sqrt{\frac{2k_B T}{N_c \omega_p^2 m}} = \frac{1}{\sin p/2} \sqrt{\frac{k_B T}{2k N_c}} \quad (45)$$

9. *Random displacements*, Equations (19) and (20):

$$\mathbf{R}_n(t) = \sum_p a_p^+ \cos(\omega_p t + \phi_p^+) \cos pn + \sum_p a_p^- \cos(\omega_p t + \phi_p^-) \sin pn \quad (46)$$

Here, the random phases ϕ^+ and ϕ^- are sampled independently of each other. For the values a_p^\pm , we utilize the ensemble average amplitudes (45), rather than sampling them randomly from the original distribution (31a).

10. *Transform Green's function* (9):

$$\hat{\mathbf{G}}(p, \alpha) = \frac{1}{\alpha^2 m + 2k(1 - \cos p)} \quad (47)$$

11. *DFT inversion* (15b) for (47) at $n=0$ and 1, accomplished by solving the integral (A12):

$$\tilde{\mathbf{G}}_0(\alpha) = \frac{1}{\alpha \sqrt{m(4k + \alpha^2 m)}}, \quad \tilde{\mathbf{G}}_1(\alpha) = \frac{2k + \alpha^2 m - \alpha \sqrt{m(4k + \alpha^2 m)}}{2k \alpha \sqrt{m(4k + \alpha^2 m)}} \quad (48)$$

12. *THK* (15a) in Laplace domain:

$$\Theta(\alpha) = \frac{\tilde{\mathbf{G}}_1(\alpha)}{\tilde{\mathbf{G}}_0(\alpha)} = \frac{(\sqrt{\alpha^2 + 4k/m} - \alpha)^2}{4k/m} \quad (49)$$

13. *THK in time domain*:

$$\theta(t) = \frac{2}{t} J_2(2t\sqrt{k/m}) \quad (50)$$

where J_2 is the second-order Bessel function. Here, the Laplace transform inversion is accomplished simply by identifying function (50) in the standard tables of Laplace transform [10, 34]. In general, inversion of the Laplace and DFTs can be accomplished numerically by utilizing algorithms (A9) and (A14).

Having obtained the random displacement vector (46) and THK (50), we proceed to the numerical simulation.

We sample the wave numbers p for (46) equidistantly from the interval $[-\pi, -\pi/2]$, $[\pi/2, \pi]$ with a step $\pi/32$. Thus, there are in total $N_c = 32$ distinct wave numbers, and this number is used to evaluate the normal amplitudes (45). The phases ϕ_p are sampled uniformly at $(0, 2\pi)$. The corresponding normal frequencies are given by (42). A time step of $\Delta t = 0.005$ was used for 20 000 steps. The atoms are given initial displacements and velocities using relationships (34) for a target temperature T . For two boundary atoms at the left and right ends of the chain lattice, the boundary conditions of type (17a) are applied. This means that displacements of these atoms, \mathbf{u}_1 and \mathbf{u}_{1001} , are enforced using a time-history of displacements of the pre-boundary atoms, \mathbf{u}_2 and \mathbf{u}_{1000} , respectively. Note that \mathbf{u}_2 and \mathbf{u}_{1000} are computed within a standard MD solver, utilizing \mathbf{u}_1 and \mathbf{u}_{1001} as dynamic boundary conditions at each time step of the simulation.

The simulation results for two target system temperatures, $T = 300$ and 600 K are shown in Figure 4. The MD system temperature oscillates about the target temperature exactly for the $T = 300$ K case. For the $T = 600$ K case, it oscillates about a value slightly higher than the target system temperature. Nonetheless, the non-linearity results in correspondingly small errors in the

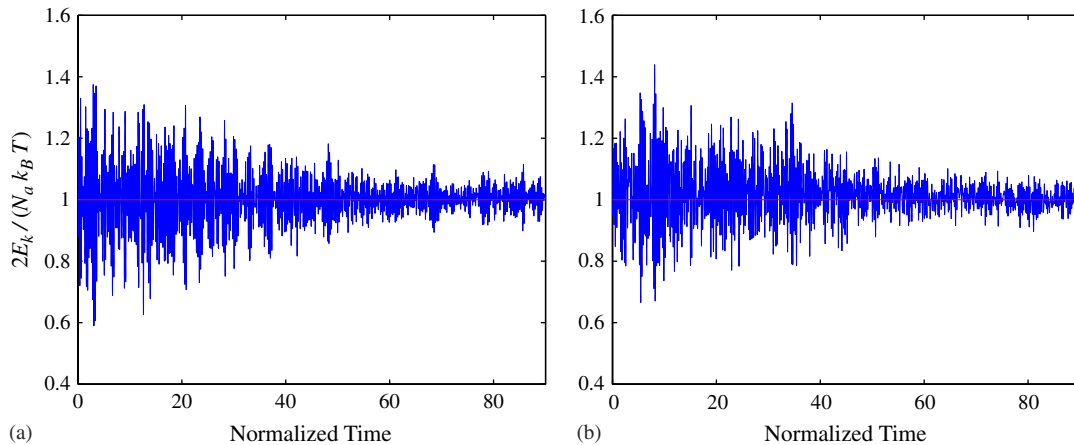


Figure 4. Temperature of a 1D lattice as a function of time within the phonon heat bath approach. Target system temperatures T_0 are: (a) 300 K; and (b) 600 K. The unit of time is $\sqrt{m/k}$.

target system temperature, where no diverging or non-controlled behaviour is observed. For the 600 K simulation, the average vibrational amplitude was 4% of the interatomic spacing, with a maximum around 20–25%; thus, the method appears accurate also in the case of moderate non-linearities.

Another important feature of these results is that no equilibration period is required for the system temperature. The system temperature starts fluctuating about the correct target value immediately. Over the course of time, the decaying amplitude of fluctuations corresponds to the free energy equilibration process; though a deeper insight into this behaviour is outside the scope of the present paper. We only note that this effect can be explained by the gradual redistribution of the kinetic energy and potential energy between all normal modes of the system due to the non-linear correlation effects. As given by Equation (33), internal energy of a harmonic lattice in thermodynamic equilibrium is comprised by the $k_B T$ increments that are identical for all normal modes.

The use of a larger number of normal modes in (20) should result in a faster minimization of the fluctuations. Indeed, Figure 5 shows the reduction in temperature fluctuations at short times in the case of utilizing 128, instead of 32, modes. These modes are sampled for the wavenumbers in the interval $[-\pi, -\pi/2]$, $[\pi/2, \pi]$ with a step $\pi/128$. Thus, for a sufficiently rich normal mode sampling, the system is close to a thermodynamic equilibrium with the heat bath, even at initial times.

5.2. Hexagonal lattice in contact with a heat source

The hexagonal lattice, as shown in Figures 2 and 3(b), is observed for the (1 1 1) crystallographic plane of a face-centred cubic (fcc) lattice. This geometry is often used in the 2D modelling of fcc metals.

Consider an orthogonal numbering of unit cells in the hexagonal lattice as displayed in Figure 3(b). Then the unit cell is represented by a single lattice atom, and the vector \mathbf{u}_n shows in-plane displacements of this atom with reference to x and y Cartesian axes: $\mathbf{u}_n \equiv \mathbf{u}_{n,m} =$

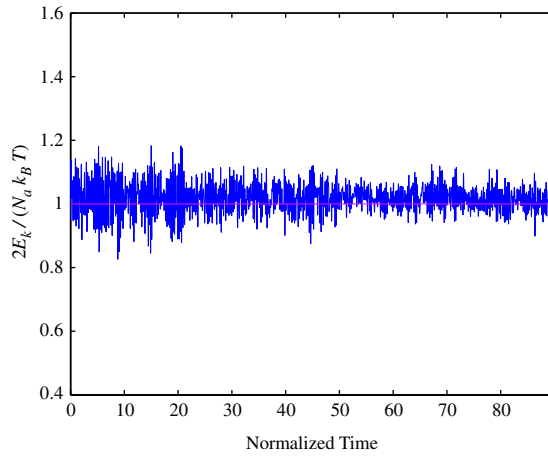


Figure 5. Phonon model at $T_0 = 600$ K; the number of normal modes is increased from 32 to 128.

$(u_{n,m}^x, u_{n,m}^y)^T$. The atomic interactions are governed by the Au Morse potential (35). Within the nearest neighbour assumption, the associate cell is formed by a symmetric group of seven lattice atoms as depicted in Figure 3.

Similar to the previous example, the potential energy of one associate cell in the hexagonal lattice can be expressed through $u_{n,m}^x, u_{n,m}^y$ and ρ . Further use of definition (5) provides seven non-zero K -matrices. We now provide a complete log of analytical results for the hexagonal lattice governed by the nearest neighbour Morse potential:

1. *Equilibrium positions and co-ordinates* of lattice atoms:

$$\mathbf{e}_{n,m} = \frac{\rho}{2} \begin{bmatrix} n \\ m\sqrt{3} \end{bmatrix}, \quad \mathbf{r}_{n,m}(t) = \mathbf{e}_{n,m} + \mathbf{u}_{n,m}(t) \tag{51}$$

2. *Potential energy* of one associate cell, Figure 3(b):

$$U = V(|\mathbf{r}_{n+1,m+1} - \mathbf{r}_{n,m}|) + V(|\mathbf{r}_{n+2,m} - \mathbf{r}_{n,m}|) + V(|\mathbf{r}_{n+1,m-1} - \mathbf{r}_{n,m}|) \\ + V(|\mathbf{r}_{n-1,m-1} - \mathbf{r}_{n,m}|) + V(|\mathbf{r}_{n-2,m} - \mathbf{r}_{n,m}|) + V(|\mathbf{r}_{n-1,m+1} - \mathbf{r}_{n,m}|) \tag{52}$$

where V is the Morse potential (35).

3. *K-matrices* (5), and the mass matrix:

$$\mathbf{K}_{1,1} = \mathbf{K}_{-1,-1} = \frac{k}{4} \begin{bmatrix} 1 & \sqrt{3} \\ \sqrt{3} & 3 \end{bmatrix}, \quad \mathbf{K}_{1,-1} = \mathbf{K}_{-1,1} = \frac{k}{4} \begin{bmatrix} 1 & -\sqrt{3} \\ -\sqrt{3} & 3 \end{bmatrix} \\ \mathbf{K}_{2,0} = \mathbf{K}_{-2,0} = k \begin{bmatrix} 1 & 0 \\ 0 & 0 \end{bmatrix}, \quad \mathbf{K}_{0,0} = -3k \begin{bmatrix} 1 & 0 \\ 0 & 1 \end{bmatrix}; \quad \mathbf{M} = \begin{bmatrix} m & 0 \\ 0 & m \end{bmatrix} \tag{53}$$

Here, the constant k is such as in (40). All other combinations of the subscript indices, such as (1, 0), (2, 1), etc., give a zero matrix.

4. *DFT (A11) of the K-matrices:*

$$\hat{\mathbf{K}}(p, q) = k \begin{bmatrix} 2 \cos 2p + \cos p \cos q - 3 & -\sqrt{3} \sin p \sin q \\ -\sqrt{3} \sin p \sin q & 3 \cos p \cos q - 3 \end{bmatrix} \quad (54)$$

5. *Normal frequencies (23).* There are in total two acoustic branches ($s = 1, 2$) for this lattice. Normal frequencies of each branch are determined by two wavenumbers, p and q :

$$\frac{m}{k} \omega_{p,q,s}^2 = 3 - \cos 2p - 2 \cos p \cos q + (-1)^s \sqrt{(\cos 2p - \cos p \cos q)^2 + 3 \sin^2 p \sin^2 q} \quad (55)$$

6. *Polarization vectors (21) before normalization:*

$$\mathbf{d}_{p,q,s} = \begin{bmatrix} 3k(\cos p \cos q - 1) + m\omega_{p,q,s}^2 \\ \sqrt{3}k \sin p \sin q \end{bmatrix} \quad (56)$$

7. *Characteristic masses (28):*

$$\mu_{p,q,s} = \frac{\mathbf{d}_{p,q,s}^T \mathbf{M} \mathbf{d}_{p,q,s}}{|\mathbf{d}_{p,q,s}|^2} = m \quad (57)$$

Obviously, this simple result is valid for any monoatomic lattice with a mass matrix of the type $\mathbf{M} = m\mathbf{I}$, where m is the atomic mass, and \mathbf{I} is a unity matrix.

8. *Normal amplitudes.* Analytical expression for the mean amplitudes is obvious from (32), (55) and (57), and we do not show it here for compactness.

9. *Random displacements (19).* Since the polarization vectors (56) are real valued for all p, q and s , we can write

$$\begin{aligned} \mathbf{R}_{n,m}(t) = & \sum_{p,q,s} a_{p,q,s}^+ \mathbf{d}_{p,q,s} \cos(\omega_{p,q,s}t + \phi_{p,q,s}^+) \cos(pn + qm) \\ & + \sum_{p,q,s} a_{p,q,s}^- \mathbf{d}_{p,q,s} \cos(\omega_{p,q,s}t + \phi_{p,q,s}^-) \sin(pn + qm) \end{aligned} \quad (58)$$

10. *Transformed Green's function.* An analytical expression can be made available by inverting the 2×2 matrix (9), where \mathbf{M} and $\hat{\mathbf{K}}$ are substituted from (53) and (54), in closed form. Meantime, such an expression is cumbersome.

The final steps (15) of the THK evaluation, in case of the hexagonal lattice, require numerical methods for the DFT and Laplace transform inversions. These methods are reviewed in the Appendix. The individual components of the resultant time-dependent function $\theta_n(t)$ was discussed and shown for different n in an earlier publication [13].

We utilize the available random displacement vector and THK for the boundary condition (17b) in application to the 2D computational problem depicted in Figure 6. This problem statement is inspired by the great potential of nanowire applications, including the Au nanowires [35], which will be used as interconnects in circuits of new generation supercomputers and NEMS devices.

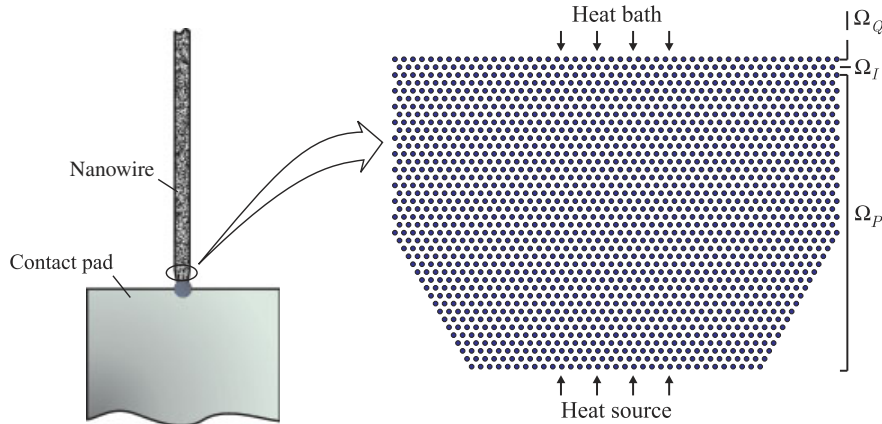


Figure 6. Left: critical region of a joint between the Au nanowire and a contact pad; right: Morse monolayer model (the actual geometry).

Critical parts of these devices are often associated with contact, joint or cross-section points that may serve also a source of heat induced by higher density of electric current in the contact area. Outside the contact area, nanowire body serves mostly as a bulk absorbent of this heat. Application of the present methodology to this type of problems is very natural. It allows reducing size of the computational domain to a small region in the vicinity of the contact, where spurious heating and probably melting of the nanowire may occur. The Au nanowire is represented by the hexagonal lattice, such as in Figures 2 and 3(b). The mechanism of heat exchange with the peripheral heat sink can be modelled by GLE boundary conditions (17b) method.

The lattice structure shown in Figure 6 (right) represents the computational domain of 1836 atoms to be studied. The principal domain Ω_P spans from the first bottom to the third top horizontal layer of atoms. The interface Ω_I is represented by the second top layer of 50 atoms corresponding to $m=0$. The first top row of atoms, at $m=1$, represents the hypothetical heat bath Ω_Q at room temperature $T=293$ K imposed by statistical properties of the random displacement term (58). Total displacements of the atoms $m=1$ are governed by (17b), and they serve as dynamic boundary conditions for the simulation over Ω_P and Ω_I . In the following discussion, the temperature will always be reported as spatially averaged over the principal region Ω_P only. Traction-free boundary conditions are applied to the left and right edges of the structure. Atomic displacements at the bottom layer, representing the contact area, are enforced in accordance with $u^x=0$ and $u^y=0.22 \sin 5t$ in order to model a friction-induced heat source.

Initial conditions are imposed in accordance with (17b) and (19) at the room temperature. For the normal mode sampling we utilize only the first ($s=1$) branch in (55)–(56), and choose p and q from the interval $[\pi/4, 3\pi/4]$ with a step $\pi/40$ resulting in $N_c=1600$ linear-independent normal modes. Heat generated at the bottom of the structure first lead to a rising system temperature, until a dynamic equilibrium, made possible due to the boundary condition (17b), is established between the principal domain and the heat bath. The equilibrium situation is reached at 8 fs after the simulation is initiated at the room temperature, Figure 7(a). The average system temperature in Ω_P at successive times is 663 K.

These results have been verified by a benchmark simulation by adding 160 additional atomic layers on top of the domain shown in Figure 6 (right), and imposing the standard zero displacement

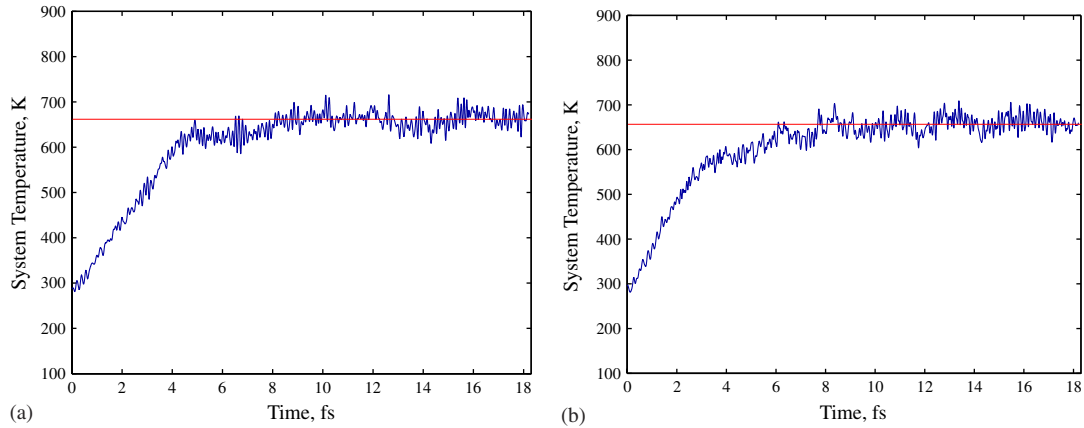


Figure 7. Spatially average temperature in the principal domain Ω_P for the lattice structure shown in Figure 6: (a) present method; and (b) benchmark solution with an explicit heat bath.

boundary conditions at the peripheral top edge of the structure. The additional layers serve as a physical thermostat for the original (smaller) system, while the benchmark model itself is not thermostatted. System temperature is still measured only in the principal region Ω_P of the same size as in the first simulation, and only for a period of time, within which the excitations imposed by the heat source do not reach the peripheral boundary of the added structure. The results are shown in Figure 7(b). This benchmark simulation shows that the dynamic equilibrium is achieved in Ω_P after 8 ps at a spatially average temperature of 657 K, which is close to the 663 K result obtained with the present method. Due to the probabilistic nature of the method, results of the computation vary slightly for different simulation runs; the results shown in Figure 7(a) and (b) represent a typical situation. As compliant with the general physics, the final (equilibrium) system temperature depends on the heat bath temperature chosen in this method. Lower heat bath temperatures, for instance, including the 0 K case ($\mathbf{R}_{n,m} = \mathbf{0}$), would have resulted in lower system temperatures due to smaller amplitudes of the constitutive normal components of the random displacement term (58), and thus smaller (or none at 0 K) input of energy to the system from the heat bath. Remarkably, the system temperature obtained exhibit similar trends, as in the work by E and Huang [22], who studied a similar 2D lattice problem with frictionally generated heat at a bottom surface, absorbing boundary conditions at the top. This fact points out on a similar physical nature of E and Huang's matching operator conditions and the present THK operator, even though these two operators adopt various mathematical forms.

5.3. Numerical strategies

Analytical results have been shown in Sections 5.1 and 5.2 for illustrative purposes only. In realistic application to complex lattice structures, a readily available quantitative form is only required for the K -matrices. All successive steps in the evaluation of the lattice spectral characteristics and THK for (19) should be accomplished numerically. A general approach to this consists of the following.

Random displacements. Create a 3D array comprised of all specific values of the wavenumbers p , q and r , which will be required later for decomposition (20) of the random vector (19); assume there are N_c elements in this array. Next, compute numerically N_c matrices $\hat{\mathbf{K}}(p, q, r)$ corresponding to all elements of the array of wavenumbers. Using these matrices, compute SN_c normal frequencies (23), polarization vectors (21), and characteristic masses (28). Then evaluate SN_c amplitudes (32), and sample independently $2SN_c$ random phases ϕ^\pm . Create a subroutine for computing the summations in (20), using the lattice site indices n , m and l and physical time t as input parameters.

THK. Create a 4D array comprised of all specific values of the wavenumbers p , q , r and Laplace parameter α , which will be required later for the purpose of numerical transform inversions for (15). For example, the inverse DFT procedure (A14) requires N wavenumbers $p = 2\pi\tilde{p}/N$, where $\tilde{p} = -N/2, -N/2+1, \dots, N/2-1$. For each element of this array, compute numerically a matrix $\hat{\mathbf{G}}(p, q, r, \alpha)$, Equation (9). Next, compute the inverse $r \rightarrow l$ DFT of this matrix at $l = 0$ and 1, and evaluate the matrices $\tilde{\Theta}(p, q, \alpha)$ (13) for all triplets (p, q, α) . Consider these matrices as values of the time-history kernel in the transform domain, and use the computational algorithms from the Appendix for the DFT and Laplace transform inversions. The DFT inversions are only required at $|n| \leq n_c$ and $|m| \leq m_c$, as follows from Equation (17c).

6. CONCLUSIONS

We have discussed a novel method to calculate the random thermal motion term $R(t)$ in the GLE [7, 9] for the atomistic solid–solid interfaces based on a normal mode decomposition. The free parameters of this decomposition have been derived consistently from the lattice stiffness parameters, with respect to temperature of the system, and characterized in a probabilistic manner on the basis of Gibbs canonical distribution. The resultant GLE, in principle, provides dynamic boundary conditions that can be utilized within a standard MD solver. These boundary conditions provide an accurate mechanism of heat exchange between the simulated domain and the outer heat bath, because the random term in the proposed form accounts automatically for the time/space correlations of the thermal noise in the periodic lattice. As a result, the phonon heat bath captures the correct interfacial behaviour of the simulated structure.

Ultimately, the method allows bringing together a small and a large crystalline domain, and model accurately the resultant *interface* within the harmonic assumption for the larger (effectively infinite) domain, which is excluded from the explicit numerical model. Such an interface is non-reflective for the elastic waves, as well as providing a thermostating for the small domain, whose interior may incorporate arbitrary non-linearities. Example simulations with Au lattice models show that the method preserves stability and correctness for moderate non-linearities at the interface.

We note the THK and the normal mode decomposition utilized within the phonon heat bath approach are unique structural characteristics. Once obtained for a given lattice structure, they can be used in solving many specific problems involving the same type of lattice. This fact comprises an advantage in terms of convenience and computational effectiveness of the present method.

The present method is also interesting within the frameworks of modern numerical methods that couple classical particle dynamics and continuum simulations, in particular, the bridging scale method [11–14, 30, 31]. Note, the ‘one-scale’ equations (2) and (17) assume that the Ω_Q region

degrees of freedom affect the Ω_p region via the random thermal term \mathbf{R} only. Accounting for the larger scale Ω_Q -to- Ω_p elastic waves in a computationally efficient manner can be accomplished using the bridging scale approach. The latter separates the scales with a projector operator technique, and incorporates the random term \mathbf{R} as a natural part of the fine scale field. Such a multiscale approach will allow for the two-way passage of long elastic waves across the interface, as well as the effect of the peripheral (continuum) boundary conditions onto the atomistic region of interest.

One interesting possibility for the future is to utilize the fact that the present approach has a capacity to control the heat bath temperature in the course of a numerical simulation. This can be performed by the varying normal amplitudes in accordance with relationship (32), where T is viewed as the *current* (time-dependent) heat bath temperature. This feature can be particularly useful in a future multiscale approach allowing heat transfer over the continuum domain with a dynamic temperature field.

Another topic left open for the future is a rigorous criterion for the reduced normal mode sampling and resultant truncation of the wave number summations in Equation (20). This criterion should utilize general physical arguments, such as the lattice free energy or the autocorrelation properties of the thermal noise.

APPENDIX A

A.1. Fourier transform

The Fourier transform is used to transform a time-dependent function into the frequency space

$$X(\omega) = \mathcal{F}_{t \rightarrow \omega}\{x(t)\} = \int_{-\infty}^{\infty} x(t) e^{-i\omega t} dt \quad (\text{A1})$$

Fourier transforms obey the time-derivative theorem

$$\mathcal{F}_{t \rightarrow \omega} \left\{ \left(\frac{\partial}{\partial t} \right)^n f(t) \right\} = (i\omega)^n F(\omega) \quad (\text{A2})$$

The inverse Fourier transform is defined as

$$x(t) = \mathcal{F}_{\omega \rightarrow t}^{-1}\{X(\omega)\} = \frac{1}{2\pi} \int_{-\infty}^{\infty} X(\omega) e^{i\omega t} d\omega \quad (\text{A3})$$

A.2. Laplace transform

The Laplace transform of a continuous function in time gives

$$X(\alpha) = \mathcal{L}_{t \rightarrow \alpha}\{x(t)\} = \int_0^{\infty} e^{-\alpha t} x(t) dt \quad (\text{A4})$$

where α is known as the complex frequency. The Laplace transform has the following valuable properties: the convolution theorem

$$\mathcal{L}_{t \rightarrow \alpha} \left\{ \int_0^t x(t - \tau) y(\tau) d\tau \right\} = X(\alpha) Y(\alpha) \quad (\text{A5})$$

and the time-derivative rules

$$\mathcal{L}_{t \rightarrow \alpha}\{\dot{x}(t)\} = \alpha X(\alpha) - x(0-) \tag{A6}$$

$$\mathcal{L}_{t \rightarrow \alpha}\{\ddot{x}(t)\} = \alpha^2 X(\alpha) - \alpha x(0-) - \dot{x}(0-) \tag{A7}$$

Here, the notation ‘0–’ stands for a value of the argument t ‘right before’ the zero point. Mathematically, $x(0-)$ and $\dot{x}(0-)$ are limits of the functions $x(t)$ and $\dot{x}(t)$, as t approaches zero from negative values.

The convolution theorem implies that the transform of a convolution integral of two functions is equal to the product of the transforms of the individual functions. The time derivative rules imply that the transform of a time derivative is equivalent to multiplication of a function by α . This property allows reducing differential equations to simple algebraic equations in the transform domain, therefore, it is useful in finding analytical solutions to the classical equations of motion; see the example below in this section.

The inverse Laplace transform is defined as

$$x(t) = \mathcal{L}_{\alpha \rightarrow t}^{-1}\{X(\alpha)\} = \lim_{b \rightarrow \infty} \frac{1}{2\pi i} \int_{a-ib}^{a+ib} e^{zt} X(\alpha) ds, \quad a, b \in \mathbf{R} \tag{A8}$$

However, this general mathematical definition is rarely used in practical applications. In some cases, the inverse Laplace transform for $X(\alpha)$, i.e. the function $x(t)$, can be found in the standard tables, such as [34].

More generally, the inverse Laplace transform can be computed numerically. One effective numerical algorithm applicable to a wide range of functions was proposed by Weeks [36]. This algorithm can be summarized as follows:

$$x(t) = e^{ct-t/2T} \sum_{\gamma=0}^A b_{\gamma} L_{\gamma}(t/T)$$

$$b_{\gamma} = \frac{2 - \delta_{\gamma 0}}{2T(A+1)} \sum_{\eta=0}^A \left(\operatorname{Re} X(\alpha_{\eta}) - \cot \frac{z_{\eta}}{2} \operatorname{Im} X(\alpha_{\eta}) \right) \cos(\gamma z_{\eta}) \tag{A9}$$

$$z_{\eta} = \frac{\pi(2\eta+1)}{2(A+1)}, \quad \alpha_{\eta} = c + \frac{i}{2T} \cot \frac{z_{\eta}}{2}, \quad T = \frac{t_{\max}}{A}, \quad c = \frac{1}{t_{\max}}$$

Here, L_{γ} are Laguerre polynomials, i is the imaginary unit, X is the Laplace transform of x ; t_{\max} is a maximum required value of the argument for the function x , and δ is the Kronecker delta,

$$\delta_{ij} = \begin{cases} 1, & i = j \\ 0, & i \neq j \end{cases} \tag{A10}$$

The value A controls the accuracy of the result, and its choice depends on t_{\max} and the behaviour of $f(t)$ at $t \in [0, t_{\max}]$. For the kernel functions considered in this and following sections of this book, a sufficient value for A is of the order 100. Weeks’s method has been found by Davies and Martin [37] to give excellent accuracy for the inversion of a wide range of functions. Other numerical inversion algorithms are discussed in [37, 38].

A.3. Discrete Fourier transform

In lattice mechanics, the DFT is used to transform functional sequences, such as the displacement vector \mathbf{u}_n or matrix \mathbf{K}_n from real space to wavenumber space.

A key issue in solving the lattice equation of motion (4) or (7) is the deconvolution of the internal force term. This is accomplished naturally with the DFT

$$\hat{x}(p) = \mathcal{F}_{n \rightarrow p}\{x_n\} = \sum_n x_n e^{-ipn}, \quad p \in [-\pi, \pi] \quad (\text{A11})$$

$$x_n = \mathcal{F}_{p \rightarrow n}^{-1}\{\hat{x}(p)\} = \frac{1}{2\pi} \int_{-\pi}^{\pi} \hat{x}(p) e^{ipn} dp \quad (\text{A12})$$

which obeys the *convolution theorem*

$$\mathcal{F}_{n \rightarrow p} \left\{ \sum_{n'} x_{n-n'} y_{n'} \right\} = \hat{x}(p) \hat{y}(p) \quad (\text{A13})$$

Here, the calligraphic symbol \mathcal{F} denotes the Fourier transform operator, and the hatted notation used for the Fourier domain function.

The inverse DFT can be computed numerically by applying a trapezoidal or midpoint scheme to the integral (A12):

$$x_n = \mathcal{F}_{p \rightarrow n}^{-1}\{\hat{x}(p)\} = \frac{1}{N} \sum_{\tilde{p}=-N/2}^{N/2-1} \hat{x}(2\pi\tilde{p}/N) e^{i2\pi\tilde{p}n/N} \quad (\text{A14})$$

Here, N is the total number of integration steps, which represents an effective size of the real space domain: $N = n_{\max} - n_{\min} + 1$, where n_{\min} and n_{\max} are the minimal maximal values of the index n utilized for (A11). In application to periodic lattices, N gives the physical size of the lattice in unit cells along the corresponding translation vector. The value \tilde{p} in (A14) is an *integer* wavenumber index, varying from $-N/2$ to $N/2 - 1$.

The nature of Fourier integrals is such that discretization procedures of the type (A14) are *exact*. Indeed,

$$\begin{aligned} \frac{1}{N} \sum_{\tilde{p}=-N/2}^{N/2-1} \hat{x} \left(\frac{2\pi\tilde{p}}{N} \right) e^{i2\pi\tilde{p}n/N} &= \frac{1}{N} \sum_{\tilde{p}=-N/2}^{N/2-1} \left(\sum_{n'} x_{n'} e^{-i2\pi\tilde{p}n'/N} \right) e^{i2\pi\tilde{p}n/N} \\ &= \frac{1}{N} \sum_{n'} x_{n'} \sum_{\tilde{p}=-N/2}^{N/2-1} e^{-i2\pi\tilde{p}n'/N} e^{i2\pi\tilde{p}n/N} \\ &= \sum_{n'} x_{n'} \delta_{nn'} = x_n \end{aligned} \quad (\text{A15})$$

Provided that the function \hat{x} is simple enough, the integral (A12) can be used for analytical inversion of the DFT. Meanwhile, solutions involving a standard summation (A14) are referred to as semi-analytical.

A final valuable property of the DFT is the *shift theorem*,

$$\mathcal{F}\{x_{n+h}\} = \hat{x}(p) e^{ihp}, \quad h \in \mathbf{Z} \tag{A16}$$

A.4. Statistical properties of the thermal noise

Vector (16a) represents a random process viewed as a combination of S random functions of time (components of this vector). This process is characterized by a vector of mean values (first statistical moment) and an autocorrelation matrix (second statistical moment). Since vector R equilibrium oscillations, a snapshot of this vector at $t=0$ provides a set of thermodynamically equilibrium initial conditions, and Equation (16a) can be rewritten as

$$\mathbf{R}_n(t) = \mathbf{M} \sum_{n'} (\mathbf{g}_{n-n'}(t) \dot{\mathbf{R}}_{n'}(0) + \dot{\mathbf{g}}_{n-n'}(t) \mathbf{R}_{n'}(0)) \tag{A17}$$

The statistical moments can be conveniently written for the time derivative of the random displacements, i.e. for the vector $\dot{\mathbf{R}}$. The ergodic hypothesis of statistical mechanics assumes equivalence of the time and ensemble averages, so that the first moment of $\dot{\mathbf{R}}$ can be written as the ensemble averages at some fixed time t :

$$\langle \dot{\mathbf{R}}_n(t) \rangle = \mathbf{M} \sum_{n'} (\dot{\mathbf{g}}_{n-n'}(t) \langle \dot{\mathbf{R}}_{n'}(0) \rangle + \ddot{\mathbf{g}}_{n-n'}(t) \langle \mathbf{R}_{n'}(0) \rangle) \tag{A18}$$

Mean values of the initial displacements and velocities are zeroes for a regular harmonic lattice, therefore,

$$\langle \dot{\mathbf{R}}_n(t) \rangle = \mathbf{0} \tag{A19}$$

For the autocorrelation matrix function, we have

$$\langle \dot{\mathbf{R}}_n(t) \dot{\mathbf{R}}_{n'}^T(0) \rangle = \mathbf{M} \sum_{n''} (\dot{\mathbf{g}}_{n-n''}(t) \langle \dot{\mathbf{R}}_{n''}(0) \dot{\mathbf{R}}_{n'}^T(0) \rangle + \ddot{\mathbf{g}}_{n-n''}(t) \langle \mathbf{R}_{n''}(0) \dot{\mathbf{R}}_{n'}^T(0) \rangle) \tag{A20}$$

where we can use (e.g. [5, 23])

$$\langle \dot{\mathbf{R}}_{n''}(0) \dot{\mathbf{R}}_{n'}^T(0) \rangle = \mathbf{M}^{-1} \delta_{n'',n'} k_B T, \quad \langle \mathbf{R}_{n''}(0) \dot{\mathbf{R}}_{n'}^T(0) \rangle = \mathbf{0} \tag{A21}$$

For a monoatomic lattice, where $\mathbf{M} = m\mathbf{I}$, m is the atomic mass and \mathbf{I} is a unity matrix, we obtain

$$\langle \dot{\mathbf{R}}_n(t) \dot{\mathbf{R}}_{n'}^T(0) \rangle = k_B T \sum_{n''} \dot{\mathbf{g}}_{n-n''}(t) \delta_{n'',n'} = k_B T \dot{\mathbf{g}}_{n-n''}(t) \tag{A22}$$

More generally,

$$\langle \dot{\mathbf{R}}_n(t + \tau) \dot{\mathbf{R}}_{n'}^T(\tau) \rangle = k_B T \dot{\mathbf{g}}_{n-n'}(t) \tag{A23}$$

A similar result was also shown by Adelman and Doll Reference [5].

Next, we can show in closed form that the normal mode decomposition (46) for the 1D collinear lattice with the nearest neighbour interaction, Figure 3, yields the same autocorrelation moment (A23) obtained for the original vector (16a). Here, time derivative of the dynamic Green's function can be derived by multiplying (47) with α , followed by the Fourier and Laplace inversion. This gives [10]

$$\dot{g}_n(t) = \frac{1}{m} J_{2n}(\Omega t), \quad \Omega = 2\sqrt{k/m} \tag{A24}$$

Employ a normal mode decomposition of $\dot{\mathbf{R}}$ for this lattice in the form

$$\dot{\mathbf{R}}_n(t) = \sum_p a_p \omega_p \cos(\omega_p t - \tilde{p}n + \phi_p) \quad (\text{A25})$$

where the unity polarization vector (21) was utilized. Here, the standing waves similar to (20) are formed by pairs of the normal modes with the opposite wave numbers and equal amplitudes.

Correlation of two arbitrary normal modes from this decomposition is given by the time average

$$\begin{aligned} A_{p,p'}(t) &= a_p a_{p'} \omega_p \omega_{p'} \lim_{t_m \rightarrow \infty} \frac{1}{t_m} \int_0^{t_m} \cos(\omega_p(\tau + t) - \tilde{p}n + \phi_p) \cos(\omega_{p'}\tau - \tilde{p}'n' + \phi_{p'}) d\tau \\ &= \frac{1}{2} a_p a_{p'} \omega_p \omega_{p'} \cos(\omega_p \tau - \tilde{p}n + \tilde{p}'n' + \phi_p - \phi_{p'}) \delta_{p,p'} \end{aligned} \quad (\text{A26})$$

Autocorrelation of the thermal noise (A25) is then a summation over all such terms (vector \mathbf{R} becomes a scalar for the present lattice model)

$$\overline{\dot{\mathbf{R}}_n(t + \tau) \dot{\mathbf{R}}_n(\tau)} = \sum_{p,p'} A_{p,p'}(t) = \frac{1}{2} \sum_p a_p^2 \omega_p^2 \cos(\omega_p \tau - \tilde{p}(n - n')) \quad (\text{A27})$$

Next, use the equivalence of the ensemble and time averages, which follows from the ergodic hypothesis of statistical mechanics, utilize amplitudes (45) and frequencies (42), replace the sum over p by an integral, and make the change variable $\bar{p} = \pi p/N$, or equivalently, $\bar{p} = \tilde{p}/2$. This gives a result, which is in agreement with the autocorrelation property (A23) of the original random term

$$\begin{aligned} \langle \dot{\mathbf{R}}_n(t + \tau) \dot{\mathbf{R}}_{n'}(\tau) \rangle &= \frac{k_B T}{m} \frac{1}{\pi} \int_0^\pi \cos(\Omega t \sin \bar{p} - 2\bar{p}(n - n')) d\bar{p} \\ &= \frac{k_B T}{m} J_{2(n-n')}(\Omega t) = k_B T \dot{g}_{n-n'}(t) \end{aligned} \quad (\text{A28})$$

Here, we used an integral definition of the Bessel function

$$J_n(x) = \frac{1}{\pi} \int_0^\pi \cos(x \sin y - ny) dy, \quad x, y \in \Re, \quad n = 0, 1, \dots \quad (\text{A29})$$

ACKNOWLEDGEMENTS

The authors are grateful for the financial support from the US National Science Foundation. Many valuable comments by Dr Dmitry Dorofeev and Dr Albert To helped to improve the technical content and presentation of this work.

REFERENCES

1. Berendsen HJC, Postma JPM, van Gunsteren WF, DiNola A, Haak JR. Molecular dynamics with coupling to an external bath. *Journal of Chemical Physics* 1984; **81**(8):3684–3690.

2. Andersen HC. Molecular dynamics simulations at constant pressure and/or temperature. *Journal of Chemical Physics* 1980; **72**(4):2384–2393.
3. Nosé S. A molecular dynamics method for simulations in the canonical ensemble. *Molecular Physics* 1984; **53**:255–268.
4. Hoover WG. Canonical dynamics: equilibrium phase-space distributions. *Physical Review A* 1985; **31**(3): 1695–1697.
5. Adelman SA, Doll JD. Generalized Langevin equation approach for atom/solid-surface scattering: general formulation for classical scattering off harmonic solids. *Journal of Chemical Physics* 1976; **64**:2375–2388.
6. Cai W, DeKoning M, Bulatov VV, Yip S. Minimizing boundary reflections in coupled-domain simulations. *Physical Review Letters* 2000; **85**:3213–3216.
7. Karpov EG, Wagner GJ, Liu WK. A Green's function approach to deriving non-reflecting boundary conditions in molecular dynamics simulations. *International Journal for Numerical Methods in Engineering* 2005; **62**(9): 1250–1262.
8. Park HS, Karpov EG, Liu WK. Non-reflecting boundary conditions for atomistic, continuum and coupled atomistic/continuum simulations. *International Journal for Numerical Methods in Engineering* 2005; **64**: 237–259.
9. Wagner GJ, Karpov EG, Liu WK. Molecular dynamics boundary conditions for regular crystal lattices. *Computer Methods in Applied Mechanics and Engineering* 2004; **193**:1579–1601.
10. Liu WK, Karpov EG, Park HS. *Nano Mechanics and Materials: Theory, Multiscale Methods and Applications*. Wiley: New York, 2006.
11. Liu WK, Karpov EG, Zhang S, Park HS. An introduction to computational nano mechanics and materials. *Computer Methods in Applied Mechanics and Engineering* 2004; **193**:1529–1578.
12. Park HS, Karpov EG, Klein PA, Liu WK. Three-dimensional bridging scale analysis of dynamic fracture. *Journal of Computational Physics* 2005; **207**:588–609.
13. Park HS, Karpov EG, Liu WK, Klein PA. The bridging scale for two-dimensional atomistic/continuum coupling. *Philosophical Magazine* 2005; **85**(1):79–113.
14. Wagner GJ, Liu WK. Coupling of atomistic and continuum simulations using a bridging scale decomposition. *Journal of Computational Physics* 2003; **190**:249–274.
15. Dupuy LM, Tadmor EB, Miller RE, Phillips R. Finite-temperature quasicontinuum: molecular dynamics without all the atoms. *Physical Review Letters* 2005; **95**(6):060202.
16. E W, Engquist B, Li X, Ren W, Vanden-Eijnden E. The heterogeneous multiscale method: a review. Preprint.
17. Qu S, Shastry V, Curtin WA, Miller RE. A finite temperature, dynamic, coupled atomistic/discrete dislocation method. *Modeling and Simulation in Materials Science and Engineering* 2005; **13**(7):1101–1118.
18. Strachan A, Holian BL. Energy exchange between mesoparticles and their internal degrees of freedom. *Physical Review Letters* 2005; **94**(1):014301.
19. Curtarolo S, Ceder G. Dynamics of an inhomogeneously coarse grained multiscale system. *Physical Review Letters* 2002; **88**(25):255504.
20. Xiao SP, Belytschko T. A bridging domain method for coupling continua with molecular dynamics. *Computer Methods in Applied Mechanics and Engineering* 2004; **193**:1645–1669.
21. Park HS, Karpov EG, Liu WK. A temperature equation for coupled atomistic/continuum simulations. *Computer Methods in Applied Mechanics and Engineering* 2004; **193**:1713–1732.
22. E W, Huang Z. A dynamic atomistic/continuum method for the simulation of crystalline materials. *Journal of Computational Physics* 2002; **182**(1):234–261.
23. Adelman SA, Doll JD. Generalized langevin equation approach for atom/solid-surface scattering: collinear atom/harmonic chain model. *Journal of Chemical Physics* 1974; **61**:4242–4246.
24. Ghatak AK, Kothari LS. *An Introduction to Lattice Dynamics*. Addison-Wesley: London, 1972.
25. Born M, Huang K. *Dynamic Theory of Crystal Lattices*. Oxford University Press: London, 1966.
26. Landau LD, Lifshitz EM. *Statistical Physics*. Pergamon Press: Oxford, 1980.
27. Mayer JE, Mayer MG. *Statistical Mechanics*. Wiley: New York, 1977.
28. Pathria RK. *Statistical Mechanics*. Butterworth-Heinemann: Oxford, England, 1996.
29. Curtin WA, Miller RE. Atomistic/continuum coupling in computational materials science. *Modelling and Simulation in Materials Science and Engineering* 2003; **11**:R33–R68.
30. Tang S, Hou TY, Liu WK. A mathematical framework of the bridging scale method. *International Journal for Numerical Methods in Engineering* 2006; **65**(10):1688–1713.
31. Tang S, Hou TY, Liu WK. A pseudo-spectral multiscale method: Interfacial conditions and coarse grid equations. *Journal of Computational Physics* 2006; **213**(1):57–85.

32. Karpov EG, Yu H, Park HS, Liu WK, Wang QJ, Qian D. Multiscale boundary conditions in crystalline solids: theory and application to nanoindentation. *International Journal of Solids and Structures* 2006, in press.
33. Harrison DE. Application of molecular dynamics simulations to the study of ion-bombarded metal surfaces. *Critical Reviews in Solid State and Materials Science* 1988; **14**(Suppl. 1):S1–S78.
34. Oberhettinger F, Badii L. *Tables of Laplace Transforms*. Springer: Berlin, 1973.
35. Kovtyukhova NI, Mallouk TE. Nanowires and building blocks for self-assembling logic and memory circuits. *Chemistry—A European Journal* 2002; **8**(9):4355–4363.
36. Weeks WT. Numerical inversion of Laplace transforms using Laguerre functions. *Journal of the Association for Computing Machinery* 1966; **13**(3):419–429.
37. Davies B, Martin B. Numerical inversion of the Laplace transforms: a survey and comparison of methods. *Journal of Computational Physics* 1979; **33**:1–32.
38. Duffy DG. On the numerical inversion of Laplace transforms: comparison of three new methods on characteristic problems from applications. *ACM Transactions on Mathematical Software* 1993; **19**(3):333–359.